MODELING PROGRESSIVE COLLAPSE IN REINFORCED CONCRETE FRAMED STRUCTURES

Khalid M. Mosalam[1], Mohamed Talaat[2], and Sangjoon Park[3]

[1] *Professor and Vice Chair, Department of Civil and Environmental Engineering, University of California, Berkeley, CA 94720-1710, U.S.A., Email: mosalam@ce.berkeley.edu*

[2] *Senior Engineer, Simpson Gumpertz and Heger Inc., San Francisco, U.S.A., mtalaat@sgh.com*

[3] *Graduate Student, Dept. of Civil & Env. Eng., Univ. of California, Berkeley, U.S.A., sangjoon@berkeley.edu*

ABSTRACT: The paper presents an analytical formulation of an element removal algorithm based on dynamic equilibrium and the resulting transient change in system kinematics. The algorithm is implemented into an open-source finite element code, is numerically validated using a benchmark problem with simple element removal criteria, and is able to capture the effect of uncertainty in member capacity. Realistic element removal criteria are introduced for mode-dependent gravity load collapse of seismically deficient and retrofitted reinforced concrete (RC) columns. An application is presented using a RC 3-bay, 3-story frame previously tested on a shaking table. In this application, comparison between the computationally predicted and experimentally observed collapse modes is presented giving confidence in the developed analytical formulation.

KEYWORDS: Collapse, Dynamic analysis, Element removal, Frame, Reinforced concrete

1. INTRODUCTION

Progressive collapse assessment using nonlinear time-history finite element (FE) simulation is gaining popularity over traditional methods based on alternate path analysis and redundancy detailing. Review of applications of these traditional methods can be found in [1]. There is limited literature on this developing field of research as few experimental investigations were conducted on reduced-scale reinforced concrete (RC) frames that are redundant enough to experience progressive collapse, with seismically deficient RC columns designed to lose axial load capacity, e.g. [2,3]. Experimental data from these studies are intended to establish the behavior of RC systems after the loss of one or more columns. However, observed collapse modes are limited and difficult to generalize to cases involving disconnection and possible subsequent collision by collapsed elements.

Several analytical approaches were developed for modeling progressive collapse [1]. To capture the progression of collapse, one must model the behavior of components under extreme loading and identify the criteria for their removal. Two modes of RC column collapse, namely shear-axial and flexure-axial, are presented. Shear-axial collapse was investigated in several experimental and analytical studies [3]. The shear friction-based model in [4] is utilized to establish limit-states for shear-axial collapse. The damage indices in [1] for fiber-discretized cross-sections are used for flexure-axial collapse. For non-ductile and retrofitted –using fiber-reinforced polymers (FRP)– columns, new models are adopted from [1] for confined fiber-discretized cross-section and confinement-sensitive concrete material, and from [1] for confinement-sensitive bar buckling and lap splices. The computational implementation was carried out in OpenSees [5]. Finally, the RC 3-bay, 3-story frame from [3] is adopted as an application of the developed computational approach for collapse modeling with element removal.

2. DIRECT ELEMENT REMOVAL: MECHANICS, IMPLEMENTATION, AND VALIDATION

Consider the dynamic equilibrium of the node in Figure 1a. At time t, beams $B1$ & $B2$ and columns $C1$ & $C2$ are attached to the node. The free-body diagram is shown without externally applied or damping nodal forces. F and M refer respectively to resisting forces (both shear and axial) and bending moments from the attached

elements. The node has a lumped translational mass m and a rotational mass moment of inertia I. Dynamic equilibrium is satisfied by the nodal inertia forces ma_x, ma_y, and $I\alpha$, where a_x and a_y are translational accelerations in the respective x and y directions and α is rotational acceleration in the $x-y$ plane.

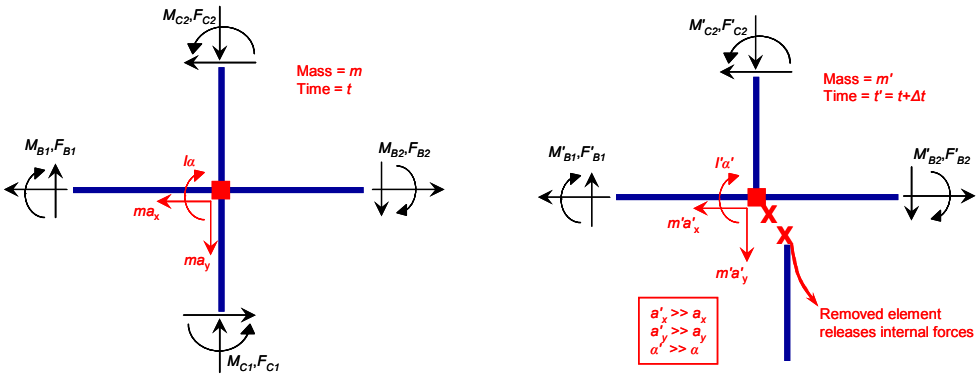

(a) Before element removal (b) After element removal

Figure 1 Dynamic equilibrium of a node connected to a collapsed element

At time t, column $C1$ reaches its collapse limit-state and is removed from the computational model at time $t' = t + \Delta t$ where Δt is the time step. The resulting free body diagram is shown in Figure 1b, where the nodal masses and accelerations are updated to m', I', a'_x, a'_y, and α', respectively. Practically, the majority of the lumped nodal masses are derived from the floor system, and the updated masses may not be significantly different from the original ones. The dynamic equilibrium of the node under resisting and inertia forces is expressed by

$$\vec{P}_{ex} + \sum \begin{Bmatrix} F_x \\ F_y \\ M \end{Bmatrix} - \begin{Bmatrix} ma_x \\ ma_y \\ I\alpha \end{Bmatrix} = \vec{P}_{ex} + \sum \begin{Bmatrix} F'_x \\ F'_y \\ M' \end{Bmatrix} - \begin{Bmatrix} m'a'_x \\ m'a'_y \\ I'\alpha' \end{Bmatrix} \tag{1}$$

where $\vec{P}_{ex}$ is vector of externally applied nodal loads, independent of the element connectivity and not affected by the removal of a collapsed element. The summation is for the elements connected at the node. Upon abrupt element collapse and removal, this dynamic equilibrium is disturbed by the sudden release of internal forces from $C1$ and must be restored before the solution continues. The resisting forces in the connected elements, $F' \,\&\, M'$, can only change as a result of updated element deformations, which require changes in relative displacements (and possibly velocities) between the elements' end-nodes. These changes result from updated nodal velocities and accelerations and do not take place instantaneously. The inertia forces are directly related to nodal accelerations a'_x, a'_y, and α', which need to change abruptly to satisfy dynamic equilibrium at time t'. Since the connected elements' end-nodes other than their shared node are under dynamic equilibrium themselves, this abrupt change is first localized at the shared node at time t'. In subsequent time steps, element removal superposes transient loading on the damaged system, whereby the resulting changes in nodal kinetics lead to an updated set of resisting (and inertia) forces propagating outward through the connected elements into neighboring nodes. These updated nodal forces must satisfy dynamic equilibrium of their respective degrees of freedom (DOFs) during every time step resulting in updated inertia forces and nodal accelerations. This process continues to propagate in the damaged system until updated nodal configurations for a new equilibrium state are reached.

Upon reaching the new equilibrium state, the nodal velocities of the damaged system result in displacement overshooting, amplifying deformation demand in the structural elements. In the hypothetical absence of external excitation, free vibration of the system ensues. An initial transient phase is followed by a steady-state phase oscillating about the new equilibrium state. The new deformation demands may lead to collapse of other elements,

which would be 'safe' in the new equilibrium state using quasi-static analysis. If so, a second transient phase is excited, and this process continues until the system either (a) reaches an equilibrium state about which it can safely oscillate and collapse progression is arrested; (b) undergoes overall gravity load collapse; or (c) undergoes partial collapse which is nevertheless compartmentalized while the rest of it survives. In case (c), the structure will probably need to be ultimately demolished, yet prospect of maintaining life safety is enhanced compared to case (b). In the presence of an earthquake excitation, the input ground motion is treated as equivalent external loads. The input time step may be larger than adequate for transient effects, particularly if reaching a new equilibrium state requires local axial vibrations in stiff structural elements with significantly short natural periods. Hence, shorter time steps are needed immediately after element removal, during which the input ground motion is interpolated. An adaptive time stepping scheme can be used for computational efficiency [1].

An algorithm is designed and implemented for automated removal of collapsed elements during an ongoing simulation, Figure 2. The implementation is carried out as a new OpenSees module, designed so that it is called by the main analysis module after each converged load step, and ordered to check each element for possible violation of its removal criteria. A violation of any criterion triggers the activation of the element removal algorithm before returning to the main analysis module. The algorithm is split into two main sets of procedures. The first set is fully implemented within the source-code of OpenSees. It includes updating nodal masses, checking if the removal of the collapsed element results in leaving behind dangling nodes or floating elements, Figure 3, which must be removed, and removing all associated element and nodal forces, imposed displacements, and constraints. The second set involves tracking motion of removed element for possible collision. The kinetics of the separated end-node(s) at the time of separation are identified from the last converged state of the system, representing the initial conditions for free falling or rotating motion of the collapsed element. This motion is tracked as a rigid body motion of the element under effects of its own weight, and compared to the position of the damaged system to determine if and when collision takes place. At the time of collision, the relative impact velocity is computed and used to determine the impact duration and the magnitude and temporal variation of impact force to be superposed on the damaged system during subsequent time steps. This second set of procedures is performed in the present study by conducting the necessary computations using MATLAB [6], and inputting the results to OpenSees.

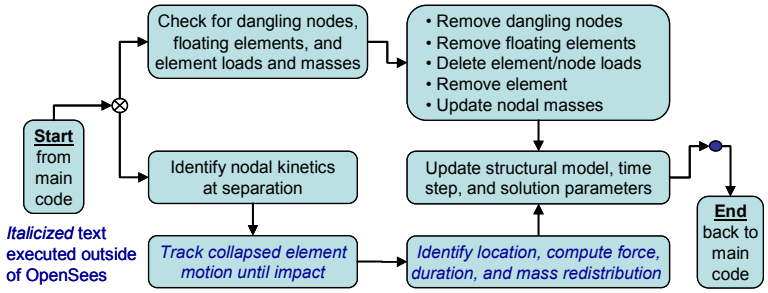

Figure 2 Automatic element removal algorithm

After completing both sets of procedures, the algorithm updates the system state to the new masses, geometry and impact forces. The assumption of Rayleigh viscous damping (mass and/or stiffness proportional) is implicitly affected. Since numerical convergence may face difficulties following extreme events, especially in softening structural systems, the solution parameters may need to be updated. This is conducted by iteratively switching solver type, convergence criteria, and other analysis options, e.g. time step, so that an ultimate failure to converge would likely take place only if the damaged structural system experiences global instability. An OpenSees input script for adaptive time stepping and solver modification is developed and used in the examples presented herein. The above algorithm implementation is numerically validated using a benchmark problem representing an idealized structural system consisting of two trussed cantilever beam canopies, Figure 4, with properties (elastic modulus, E, cross-sectional area, A, and moment of inertia, I) in Table 1. The truss members are linear elastic up to axial load F_y, then become either brittle or perfectly plastic up to a ductility limit, Table 2, before removal. Four cases are used to explore sensitivity of the algorithm to uncertainty in element capacities. The beam elements are linear elastic. Nonlinear geometry and large deformation effects are included in the FE model by co-rotational geometric transformation [5]. Masses are lumped as 10 ton at node 1, 6 ton at node 8, and 4 ton at nodes 6, 7, and

9-11. Gravity loads are applied followed by excitation at nodes 2-5 and 12 in the vertical direction using the earthquake record from Northridge 1994, Tarzana, 90° component, with scaled peak ground acceleration of 1.04g. A time step of 0.005 sec is chosen with no viscous damping. Collapsed truss elements separate from the structural system at the connection with the beams. Hence, collapsed element 3 falls and collides with the lower canopy at node 9. After collision, element 3 deforms in flexure as simply supported at nodes 4 and 9. The energy of the impact dissipates during one half-cycle of flexural deformation before rapidly decaying, e.g. due to friction, and element 3 remains supported by nodes 4 and 9 until collapse of the lower canopy. Collision with (or loss of) a truss element at any node results in updating this node's mass and gravity load by adding (or subtracting) 2 tons.

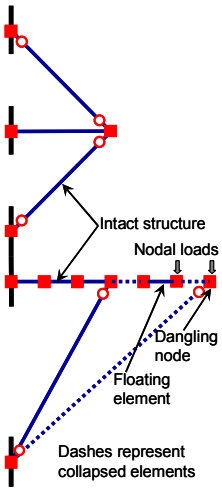

Figure 3 Elements, nodes, and loads requiring removal due to element removal

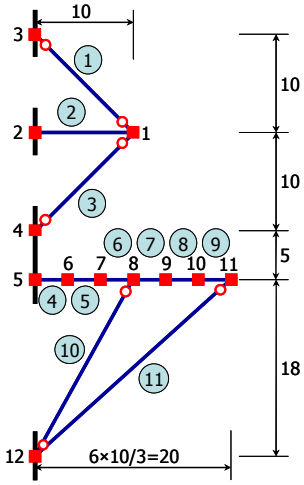

Figure 4 Geometry (in meters) and FE model of benchmark problem

Table 1 Element properties of benchmark problem

Element	EA [kN]	EI [kNm^2]	F_y [kN]
1	2,000	3,000	100
2	100,000	5,000	∞ (Elastic)
3	1,000	1,000	50
4-9	100,000	10,000	∞ (Elastic)
10,11	3,000	5,000	150

Table 2 Ultimate truss element ductility limits for benchmark problem

Truss element	Case 1	Case 2	Case 3	Case 4
1, 11	5	5	5	5
3	5	5	1	1
10	5	1	5	1

All simulations were successfully conducted without exhibiting numerical convergence problems. Cases 1 and 2 result in similar responses where no element collapse takes place. In both cases, the upper canopy elements 1 and 3 exhibit brief yielding, inducing a ductility demand of 1.17 and 1.11, respectively. Cases 3 and 4 result in collapse of element 3 onto the lower canopy at 8.875 sec. As a result, the ductility demand on element 1 increases to 2.1 and the upper canopy exhibits no further collapse. The collapse of element 3 results in larger permanent displacement in the vertical direction at node 1, Figure 5a where nodal displacements are normalized using respective values caused by the gravity load. In the lower canopy, element 3 collides with node 9 at 11.26 sec, and the resulting demand causes yielding in elements 10 and 11. In Case 3, the ductility capacity in both elements is sufficient to prevent the progression of collapse in the system, which reaches a new equilibrium state, Figure 5b. In Case 4, brittle element 10 collapses at 12.37 sec. Shortly afterwards, element 11 reaches its ultimate ductility limit and collapses at 14.57 sec leading to complete collapse of the lower canopy, Figure 5b. The deformed shapes are illustrated in Figure 6. There is clear contrast between the small difference in ductility demands for elements 3

and 10 and the large difference in simulated progressive collapse outcome. This highlights the sensitivity of the simulation procedure, due to path dependency, to uncertainty in the structural model parameters. Hence, simulation-based progressive collapse assessment needs to be conducted within a probabilistic framework [1].

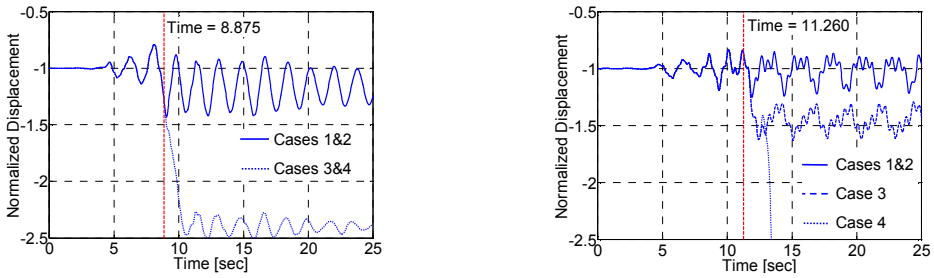

(a) Node 1 (b) Node 11

Figure 5 Simulated nodal displacement time-histories for benchmark problem

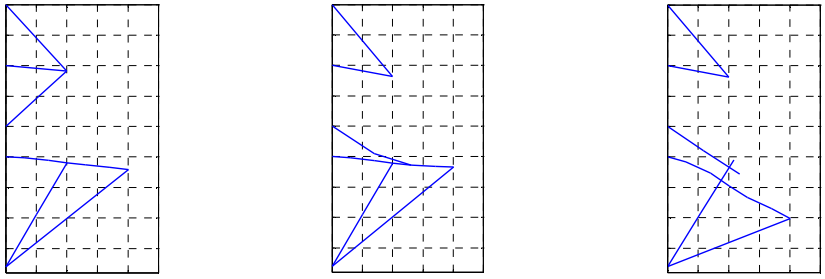

(a) Cases 1&2 (b) Case 3 (c) Case 4

Figure 6 Snapshots of benchmark structural model deformation (no amplification) at Time=14.5 sec

3. ELEMENT REMOVAL CRITERIA

Three element removal criteria are defined for two different modes of failure in seismically deficient and retrofitted RC beam-columns and for truss members. These criteria are implemented in OpenSees for force-based and displacement-based distributed plasticity fiber elements, lumped plasticity beam-column elements with fiber-discretized plastic hinges, shear-axial coupled spring elements [4] and truss elements.

A set of material damage indices is developed and calibrated in [1] for fibers presenting reinforcing steel bars, lap-spliced bars, and concrete (confined and unconfined). These damage indices are based, respectively, on the accumulation of steel plastic strains, the maximum bond-slip displacement, and the ratio of hysteretic energy dissipation to compressive fracture energy. These material-level damage indices define the following two aggregated cross-section damage indices to reflect respective loss of axial load and bending moment capacities.

$$D_A = 1 - \mathrm{I}_{\mathrm{conf}} \left(1 - \sum_{\mathrm{fibers}} \left(D_{\mathrm{fiber}} \, A_{\mathrm{fiber}} \, / A_{\mathrm{cross\text{-}section}} \right) \right), \qquad D_M = 1 - \mathrm{I}_{\mathrm{conf}} \left(1 - \sum_{\mathrm{fibers}} \left(D_{\mathrm{fiber}} A_{\mathrm{fiber}} h_{\mathrm{fiber}}^2 \, / I_{\mathrm{cross\text{-}section}} \right) \right) \qquad (2a,b)$$

where A and I refer to transformed area and moment of inertia, and h to the distance between the fiber's center and the uncracked section centroid. $0 \le D_{\mathrm{fiber}} \le 1$ is the material damage index defined for individual fibers [1]. $\mathrm{I}_{\mathrm{conf}}$ is a loss of confinement indicator with 0.0 value if confining medium (e.g. transverse reinforcing ties or FRP jacket) fracture is detected and 1.0 otherwise. These damage indices are suitable for use with deficient and FRP-retrofitted RC columns. When $D_A = 1$, the associated column cross-section is considered to have lost its axial load capacity and the element removal algorithm is invoked. A future extension may explicitly reflect the axial load level in the column. An analogous approach can be defined for D_M, but is not of interest in this paper.

An element removal criterion is developed to correspond to violating limit equations for the drift capacity model in [4] where shear-axial coupled springs are connected in series to a beam-column element to construct a compound element. When the axial limit curve is reached in a RC column, the corresponding spring is removed. Consequently, the connectivity between the associated beam-column element and the structural system is severed at one end-node. Similarly, when the shear limit curve is reached in a RC beam, the corresponding spring is removed. Hence, a shear-damaged RC column is allowed to maintain its axial load while shedding shear force until it reaches the axial load-lateral drift limit-state, while a shear-damaged RC beam is assumed to collapse in a brittle manner due to absence of a compressive axial force that may prevent shear failure from rapid propagation.

A simple element removal criterion is developed for violating maximum (positive) or minimum (negative) axial deformation values. When the axial deformation in a truss element reaches either threshold value defined by the analyst, the element is removed. The choice of such values enables modeling both brittle and ductile behavior [1].

4. RC 3-BAY, 3-STORY FRAME APPLICATION

The structural system is selected to take advantage of existing data from a shaking table test conducted at UC Berkeley. This 2D RC 3-bay, 3-story frame structure was constructed to examine the behavior of a non-ductile RC office building typical of the 1960s and 1970s designs in California. The test frame was 1/3-scale of a prototype structure, Figure 7a. Two of the columns in the frame had non-ductile details with widely spaced ties, and 90° hooks, while the other two columns followed ACI318-2002 requirements [7]. Beam designs were based on the weak-column strong-beam mechanism using beams with increased depth. Thus, joint shear stresses were effectively decreased. The dimension and reinforcement of each column were identical along all stories and those of beams were the same over all floors and spans. Summaries of the geometrical and material properties are given in Tables 3 and 4, respectively. Complete details of the frame design and test results are given in [3].

A corresponding FE model, Figure 7b, is developed and used to perform the collapse analysis. The main objective of this analysis is investigating the collapse mode, causes, and sequence. Displacement-based beam-column elements for the RC frame and zero length elements of coupled shear-axial limit state material [4] at the bases of the two columns to the east in all stories comprised the FE model. In Figure 7b, springs are shown only at the foundation level for clarity. Meshing, fiber-discretization, and constitutive modeling are similar to those of applications A and B in [1]. Nodes 1-4 are fully restrained and masses and gravity loads are lumped at the nodes. Co-rotational geometric transformation is used for all elements. The accuracy of the FE model is verified by comparing the first three periods of vibration from the analysis to those from the snap-back tests [3]. From Table 5, the maximum difference of 15% is mainly due to differences in real concrete material stiffness and that used in the simulation. Mass- and stiffness-proportional viscous damping (ζ=0.05) is assumed for the first and third modes.

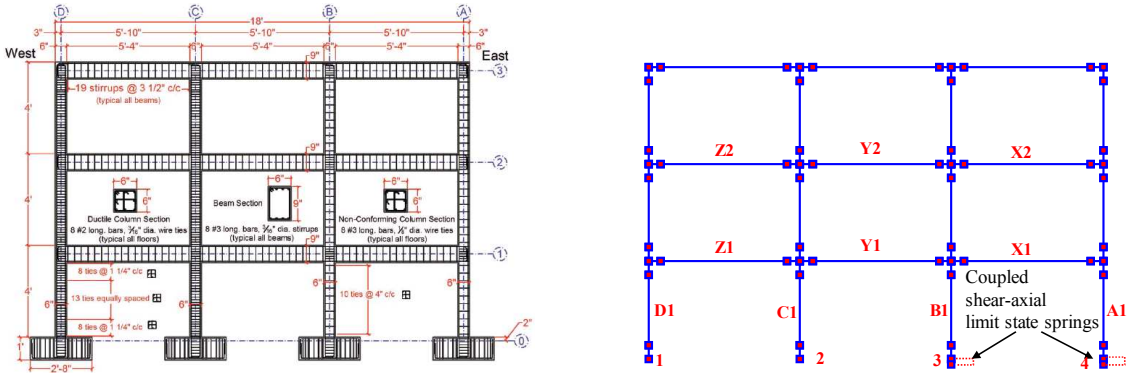

(a) 1/3 scale Test frame [3] (b) OpenSees modeling

Figure 7 Shaking table test frame and OpenSees FE model

For the purpose of this application, the ground motion recorded from the frame footings during the first run of the shaking table test is used as the reference ground motion in the analysis. This motion was the Chile

earthquake record at Valparaiso, 1985, scaled up by a factor 4.06. To induce collapse of columns A1 and B1, this scaled up ground motion needed to be scaled further by a factor of 1.43, i.e. total scale of 4.06×1.43=5.8, in the third run of the shaking table test [3]. It is to be noted that the shaking table test was performed in three runs and the third (collapse level) run took place on the damaged state from the first two runs without any repair. Therefore, a higher additional scale factor of 2.0, i.e. total scale of 4.06×2=8.12, is needed in the computational study to cause the collapse mechanism of the frame as the initial damage was not incorporated in this analysis.

Table 3 Geometry and details of shaking table test structure [3]

Structural member		Dimensions [mm]	Main reinforcement	Closed ties or stirrups
Column	Ductile	152×152	Eight 10-mm (#3) bars	3.2-mm wire@32mm overall height
	Non-ductile	152×152	Eight 6-mm (#2) bars	3.2-mm wire@100mm overall height
Beam		152×229	Four 10-mm (#3) bars top & bottom	3.2-mm wire@89mm overall span

Table 4 Material properties of shaking table test structure [3]

Material property	Concrete f_c' [MPa]	Concrete f_t' [MPa]	Concrete cover[mm]	Steel bars yield stress f_y [Mpa]			$E_{s,\text{average}}$ [Mpa]
				10-mm	6-mm	3.2-mm	
Value	25	2.7	17	441	483	655	1.85×10^5

Table 5 Comparison between analysis and snap-back test results of the shaking table test structure

Period	T_1 [sec]	T_2 [sec]	T_3 [sec]
Analysis	0.348	0.113	0.069
Snap-back test	0.303	0.101	0.069
Ratio	1.15	1.12	1.00

.

The simulated system response eventually exhibits global collapse due to soft first story mechanism after axial failure of the two non-ductile columns. In Figure 8, the story drift ratio is the average drift ratios from the four pairs of nodes defining story columns. Columns A1 and B1 are subjected to shear failure in the interval 7.5-8.0 sec yet are still carrying axial loads. At 17.14 sec, shear-damaged column A1 loses its axial load capacity and is removed, closely followed by B1 removal, and the first story drift ratio disproportionately increases compared to the third story. Subsequently, the first story beams act as a cantilever and bending moment is localized at the top of column C1 resulting in beam Y1 collapse due to loss of confinement [1] and shortly followed by the second story beam Y2 collapse. Finally, the frame completely collapses after removing the last two columns in the first story, i.e. C1 and D1. The time at incipient collapse is the time when unrestrained motion is initiated at 17.165 sec (removal of B1), and the maximum "meaningful" first story, third story, and overall drift ratios prior to this incipient collapse are 0.0472, 0.0120, and 0.0425, respectively. The mode and sequence of collapse are given in Table 7. Figure 9 compares the analytical and experimental collapse modes at their inceptions.

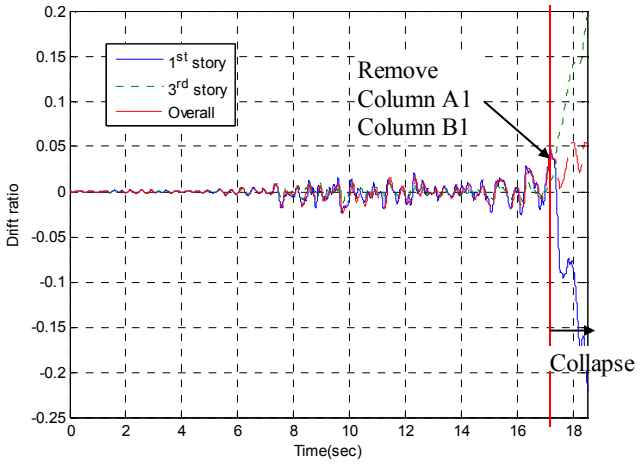

Figure 8 Drift ratio time histories obtained from the OpenSees FE model

Table 6 Comparison of computationally simulated and experimentally observed sequence of collapse

	Computation						Experiment	
Collapse mode	Shear-axial		Flexural (confinement) loss				Shear-axial	
Collapsed FE	A1	B1	Y1	Y2	C1	D1	B1	A1
Time [sec]	17.1400	17.1650	17.6160	17.9732	18.1132	18.3794	Run 1†	Run 2†

†Scale = 4.06 causing shear failure but loss of gravity load capacity took place in run 3 (scale = 5.8) [3]

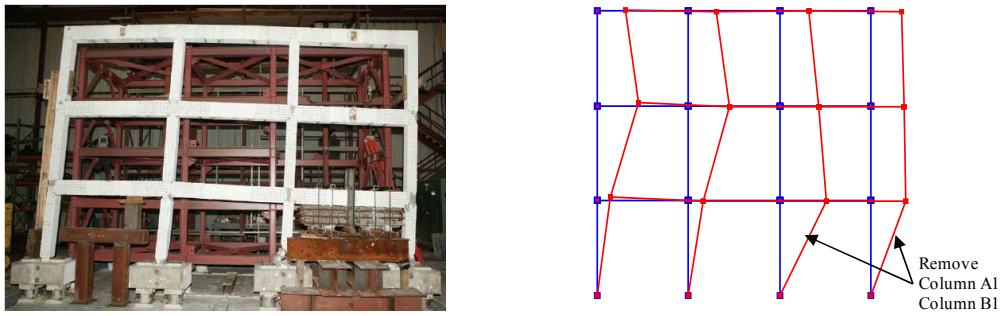

(a) Test collapse mode [3] (b) Analysis collapse mode

Figure 9 Comparison of collapse mode

7. CONCLUDING REMARKS

An analytical formulation is developed based on the dynamic equilibrium of forces to account for abrupt removal of collapsed elements from a structural model. The algorithm simulates the dynamic redistribution of forces in addition to a simplified modeling of impact. It is implemented and numerically validated using a benchmark problem. Element removal criteria are introduced for mode-dependent axial load collapse in reinforced concrete columns and for truss members. An application is presented using a RC 3-bay, 3-story frame with light transverse reinforcement. Comparisons between the computationally estimated and experimentally observed from previous shaking table tests for the collapse modes and results revealed the validity of the developed computational approach of progressive collapse simulation using direct element removal.

8. ACKNOWLEDGEMENTS

This study was supported by the Earthquake Engineering Research Centres Program of the NSF under award #EEC-9701568 and by the NSF award #0618804 through the Pacific Earthquake Engineering Research Center (PEER). Opinions and findings are those of the author(s) and do not necessarily reflect those of the NSF.

REFERENCES

1. Talaat M. and Mosalam KM. (2008). Computational modeling of progressive collapse in reinforced concrete frame structures. *PEER Technical Report* 2007/10.
2. Kim Y. and Kabeyasawa T. (2004). Dynamic test and analysis of an eccentric reinforced concrete frame to collapse. *13th World Conference on Earthquake Engineering*, Vancouver, BC, Canada.
3. Ghannoum W. (2007). Experimental and analytical dynamic collapse study of a reinforced concrete frame with light transverse reinforcements. *PhD Dissertation*, University of California, Berkeley.
4. Elwood K.J. and Moehle J.P. (2005). Axial capacity model for shear-damaged columns. *ACI Structural Journal*, ***102:4***, 578-587.
5. Mazzoni S., McKenna F., Scott, M. and Fenves, G. (2006). OpenSees User Command-Language Manual. http://opensees.berkeley.edu/OpenSees/manuals/usermanual/index.html.
6. The MathWorks, Inc. (2007). Getting Started with Matlab 7 (Release 2007b). Natick, MA.
7. ACI. (2002). Standard building code requirements for reinforced concrete. ACI 318-02. Detroit, MI.